Conceptual Design of a Helical Undulator for a TESLA SASE FEL

J. Bahrdt, A. Gaupp, U. Englisch, W. Frentrup, M. Scheer

October 24, 2000

1 Introduction

The production of circular polarization within the energy range of 500-3000 eV has to be done with a helical undulator. Above 3 keV the light of a planar undulator can be converted to circularly polarized light with quarter wave plates.

In this paper we discuss some design issues for a helical undulator which covers the energy range between 500-3000 eV at an electron energy of 23 GeV. The design is based on the technology of the BESSY II helical devices. Other technologies might be also applicable but will not be considered here. At BESSY II two helical double undulators are already in operation and 2 more helical devices are currently under construction [1].

2 Spectral Performance

Compared to other planar helical undulator designs the APPLE II [2] design provides the highest horizontal fields. Due to this reason the APPLE II has become the standard device for the production of circularly polarized light in many laboratories (ALS, BESSY, ELETTRA, ESRF, PLS, SPRING 8, SRRC, SSRL). The APPLE II design originates from a standard Halbach I undulator by cutting the magnetic arrays in longitudinal direction. Two diagonal rows are moveable by $\pm\lambda/2$ and two are fixed. The state of polarization can be controlled by shifting the rows.

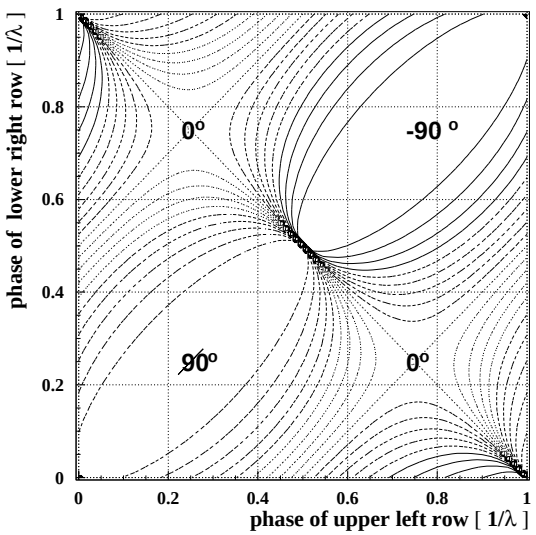

Figure 1: Relative phase between horizontal and vertical field component of an APPLE II undulator versus row phases.

Fig. 1 summarizes the various operation modes of an APPLE II undulator. Based on a simple analytical model ([1]) the relative phase difference between the horizontal and vertical fields have been derived. For a parallel row movement in one direction the phase advance is always 90 deg. Horizontally, circularly and vertically polarized light is emitted depending on the shift value which is adjustable betwen $-\lambda/2$ and $+\lambda/2$. In case of an antiparallel movement the phase advance is always zero and linearly polarized light with arbitrary declination angles between 0 and 90 deg are produced. Fig. 2 demonstrates for the case of the BESSY II UE56 the dependence of the effective B-field on the shift value. The tunable energy range is largest for the horizontal linear mode and decreases going to the vertical linear mode (shift=$\lambda/2$). In the antiparallel operation a minimum of B_{eff} shows up at a declination angle of 45 deg. At this point the tuning range is the smallest.

The helical (elliptical) radiation of the first (third) harmonic have been analyzed with a VUV-polarimeter [3] and within the measurement uncertainty the measurements agree with an analytical model [4]

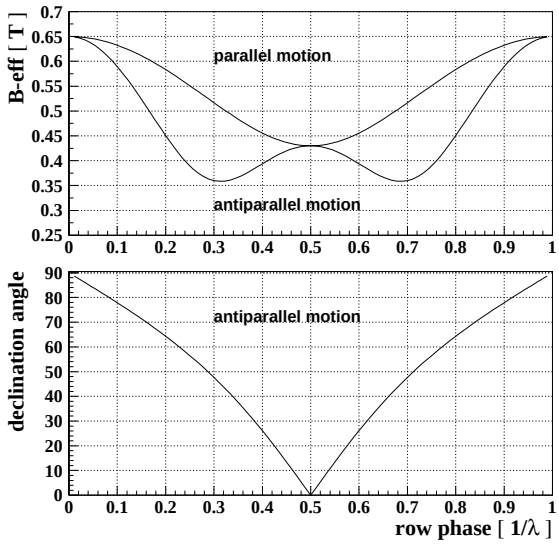

Figure 2: Top: effective fields for various row phases for parallel and antiparallel row motion. Bottom: angle of declination for antiparallel row motion versus row phase.

3 Magnetic design

To provide an energy range of 0.5-3 keV with the first harmonic at a 23 GeV electron beam a period length of 107 mm has been chosen The K-values extend from 3.7 to 9.6. Over a wide parameter range ($0.1 \leq \text{gap}/\lambda \leq 1.0$) the maximum field values on axis can be estimated from simple equtions [5]. For a detailed field analysis 3D calculations using the code RADIA [6] have been performed. To achieve high fields transverse magnet block dimensions of $\lambda/2 \cdot \lambda/2$ have been chosen. A rather conservative remanence of 1.20 Tesla which guarantees high coercive forces has been used. A 1 mm air gap between the movable rows is introduced for safety reasons. These parameters are only a guide line and may be modified in the finaL design.

The maximum horizontal and vertical fields versus phase and gap are plotted in fig. 3. The crossing points of the horizontal and vertical fields indicate the shift values for circularly polarized light. Obviously, this shift value depends on the gap and hence, during an energy scan the rows have to be moved in addition to the gap in order to keep the state of polarization fixed. The gap dependence of

the crossing point is weaker for the SPRING 8 design which consists of 3 upper and 3 lower magnetic rows where the outer rows produce the horizontal field and the central row the verftical field [7]. This design, however provides less horizontal field.

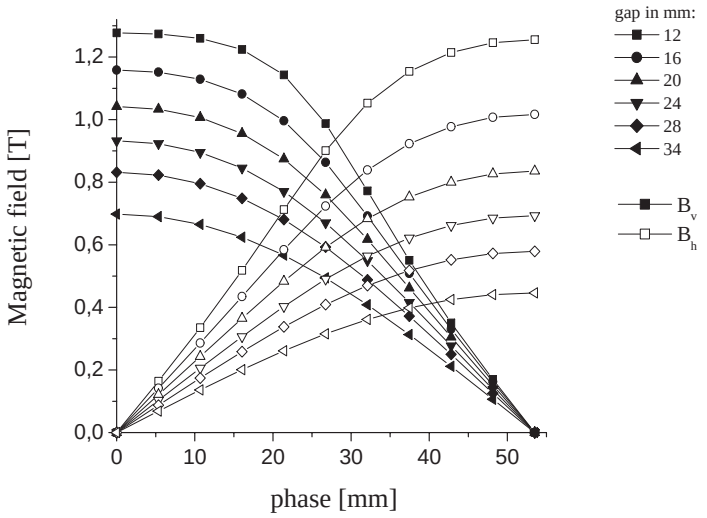

Figure 3: Horizontal and vertical fields versus gap and shift

Due to the small ratio gap/λ at smallest gap a large 5th harmonic shows up (fig. 4 and tab. 1). The maximum and the effective fields depend on the Fourier components B_i as follows:

$$\begin{aligned} B_{eff} &= \sqrt{B_1^2 + B_3^2/3^2 + B_5^2/5^2 + ...} \\ B_{max} &= B_1 + B_3 + B_5 + ... \end{aligned}$$

state of polarization	B_{max} (Tesla)	B_{eff} (Tesla)
vertical field	1.158	1.188
horizontal field	1.017	1.020
circular field	0.783	0.772

Tab. 1: Comparison of effective and maximum fields at lowest gap of 12 mm.

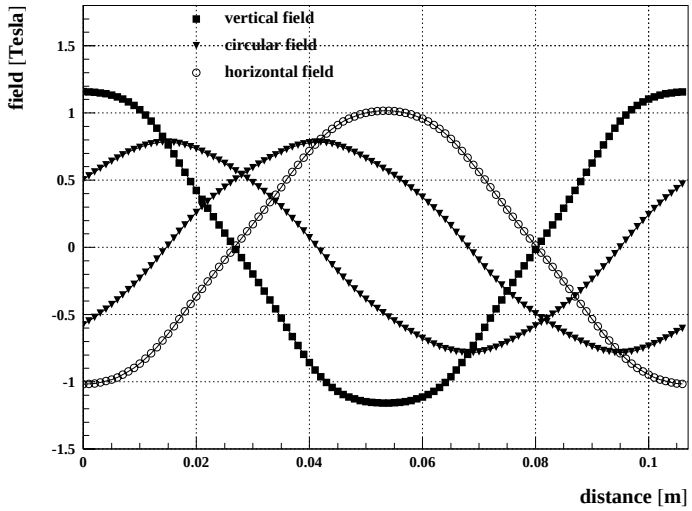

Figure 4: Horizontal, vertical and circular fields versus longitudinal coordinate

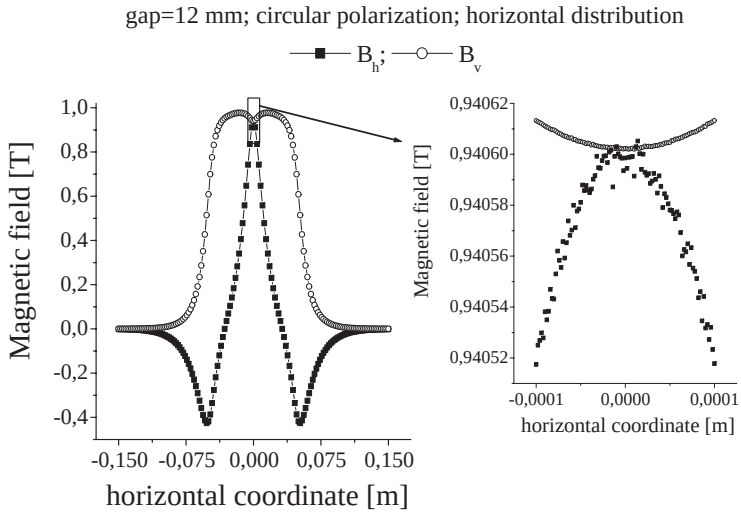

Figure 5: Transverse field distribution of horizontal and vertical fields at 12 mm gap for the heliocal case

The transverse field distribution of the APPLE II undulator is quite different from the distribution of a planar device (fig. 5): The air gap between the rows cause a local minimum of the vertical field on axis. The horizontal field decreases rapidly off axis. Nevertheless, the good field region, defined as $\Delta B/B \leq 1.e-4$, extends over $\pm 100 \mu m$, and the electron beam ($4\sigma_e$) remains completely inside the good field region for the assumed electron beam size of $\sigma_e = 20 \mu m$. The strong field roll gives a number for the required alignment tolerances.

Planar devices focus the electron beam in the vertical direction which is commonly known as edge (or natural) focussing. The APPLE II device defocusses in the vertical plane and in addition a significant focussing is observed in the horizontal plane. The focussing effects are gap and shift dependent. The strongest effects are expected for lowest gap (fig. 6). Recently, at the ESRF special shims have been developped which reduce the focussing effects of the APPLE II undulator [8]. The promising results justify a further detailed optimization for the device discussed in this paper though the effects are smaller compared to a 3^{rd} generation light source.

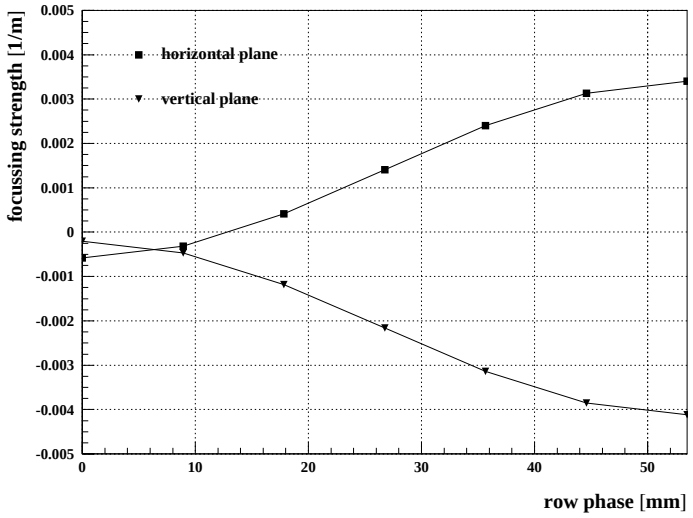

Figure 6: Focussing properties of the 107 mm APPLE II undulator at a gap of 12 mm

A large variety of extremities have been realized so far. Optimization criteria such as a kick and displacement free trajectory, minimum stray fields, maximum number of full poles and minimum field integral changes during gap and shift drive

(these changes are due to the non unity of μ) can not be fulfilled simultaneously. At the ESRF an endpole sheme has been developped which shows a low kick dependence on gap and shift motion [9].

4 Field Quality

For a SASE undulator which operates at the fundamental the tolerances on phase errors are relaxed (15 deg.) whereas the tolerances of trajectory errors are tight (trajectory wander over 5 m smaller than 20% of beam width). This can not be achieved without sorting and shimming of the magnets. Today, magnet blocks with easy axis erros below 0.4% and dipole orientation erros below 0.2 deg. can be produced for acceptable prices. However, block inhomogeneities can still not yet be controlled during fabrication. The field quality of an APPLE II undulator is very sensitive to inhomogeneities since the electrons see the field at the block edges which can not be described with the commonly used north south pole effect. Two strategies can be applied to start the final shimming from an already good field quality. The fabrication process can certainly be improved since many magents show systematic inhomogeneities which mirror the field inhomohgeneities during pressing. On the other hand, the transverse distribution of the horizontal and vertical field integrals of the individual magnets can be measured with a streched wire system and used in a subsequent sorting procedure [1].

In any case a shimming of the assembled structure will be unavoidable. Conventional shimming techniques (placing of soift iron shims on top of the magnets) are difficult because the shims would not stay in place during row shift without gluing and right at the undulator axis no shims can be placed. Therefore, another technique, called virtual shimming, is now used as a standard operation [10] in several laboratories. Vertically magnetized blocks are moved in horizontal or vertical direction producing vertical or horizontal fields on axis (fig. 7). In principle, phase shimming can be done moving horizontally magnetized blocks. This knob, however will not be needed in a SASE undulator due to the relaxed phase tolerances and hence, for mechanical simplification two magnets can be mounted into one magnet keeper. Lamellated spacers are commercially available and can be used to adjust the transverse position of the keeper (fig. 8)

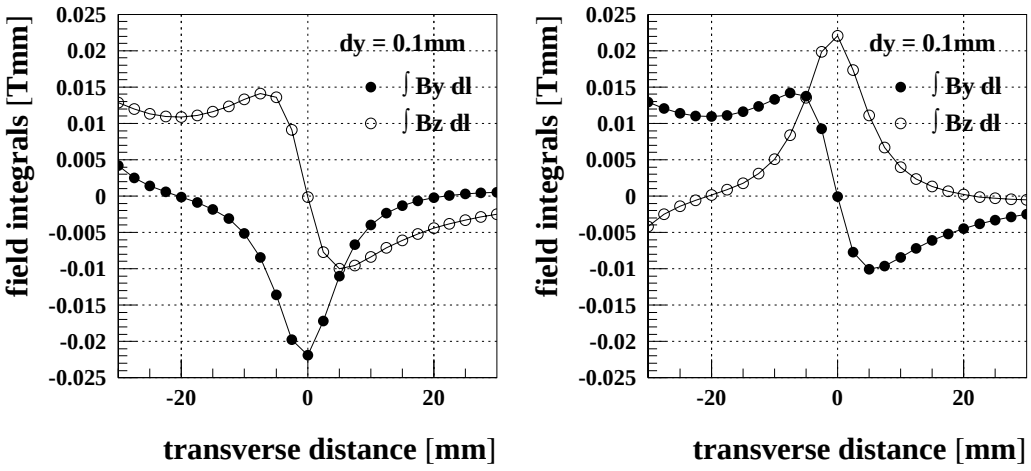

Figure 7: Field integral variation for horizontal and vertical block movement

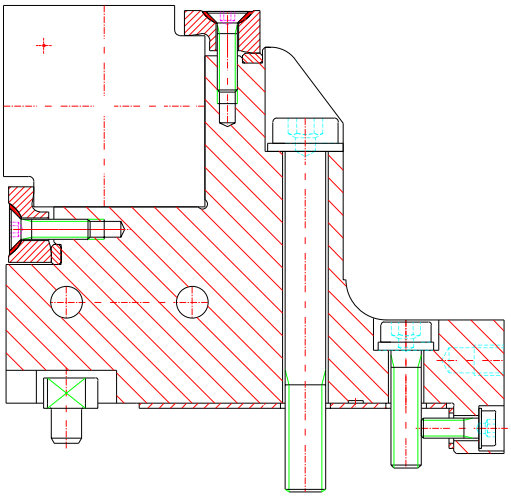

Figure 8: Layout of a magnet keeper (not to scale). 1 mm lamellated spacers for virtual shimming are provided.

5 Mechanical Considerations, Drive system

In contrast to the VUV-SASE FELs an X-ray FEL has large β-functions of a few 10 m. This allows separated function devices (no integrated focussing inside the undulator) with undulator module lengths up to to 5 m. This length can be filled up with either two I-beams separated by an air gap of only a few 0.1 mm (BESSY II solution for the long planar devices, a similar approach is realized at SPRING 8) or with a single I-beam. The latter alternative reduces the costs for the drive system by a factor of two. On the other hand a long I-beam is more sensitive to bending due to magnetic forces and vertical temperature gradients.

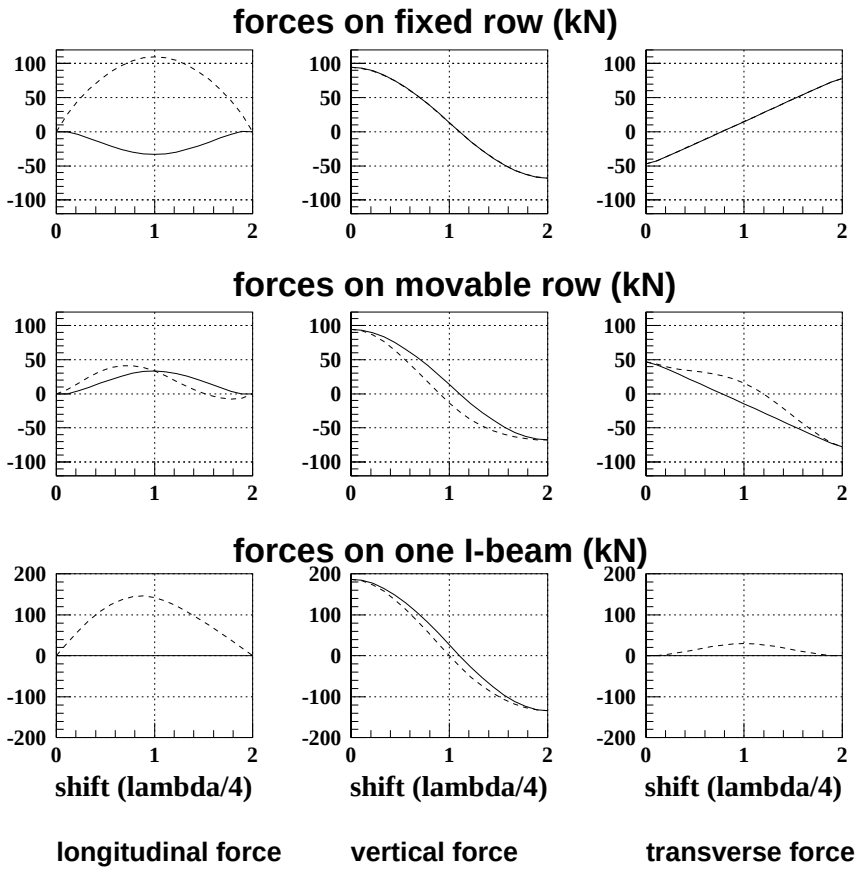

Figure 9: Forces on the individual rows and one I-beam for the parallel (solid line) and antiparallel motion (dashed line) at a gap of 12 mm.

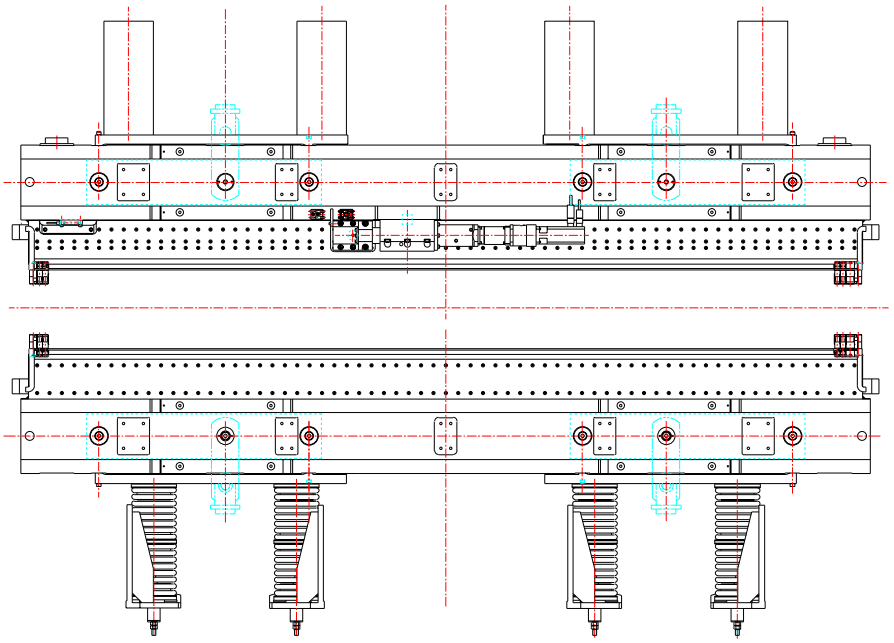

Figure 10: I-beams of the BESSY II UE46 undulator

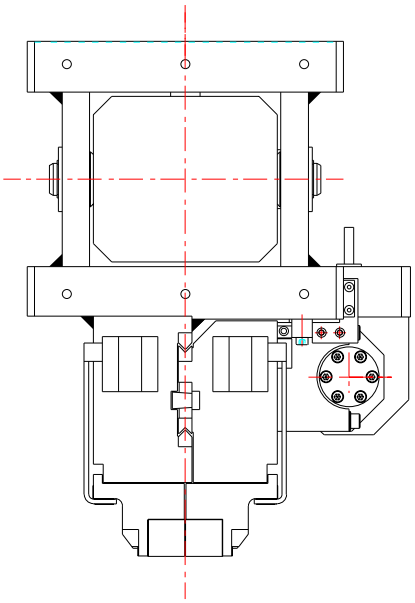

Figure 11: Cut of the UE46 I-beam

The forces seen by the individual rows and one I/beam are plotted in fig. 9. The vertical forces of 18 to can be handled if the I-beam is supported at four locations as it is planned for the BESSY II UE46 device. The vertical forces change sign during row shift. The I-beams of the BESSY II devices are preloaded with springs (lower I-beam) and blocks of lead (upper I-beam) to avoid an undefined "jump" of the I-beam due to sign reversal of the vertical force during row shift (fig. 10). This concept might not be applicable in the antiparallel mode in view of the strong repelling forces of 10 to. However, the gap can be kept constant when the vertical drive system in running in feed back loop during row shift. The transverse forces between the rows are of the order of 1-1.5 to/m which can be taken by commercial linear bearings as used in the BESSY II IDs (fig. 11). For the antiparallel mode strong longitudinal and transverse forces between the upper and lower I-beam show up which have to be considered constructing the joint between the I-beam and the girder. The longitudinal force between the rows of 12 to define the layout of the longitudinal drive system.

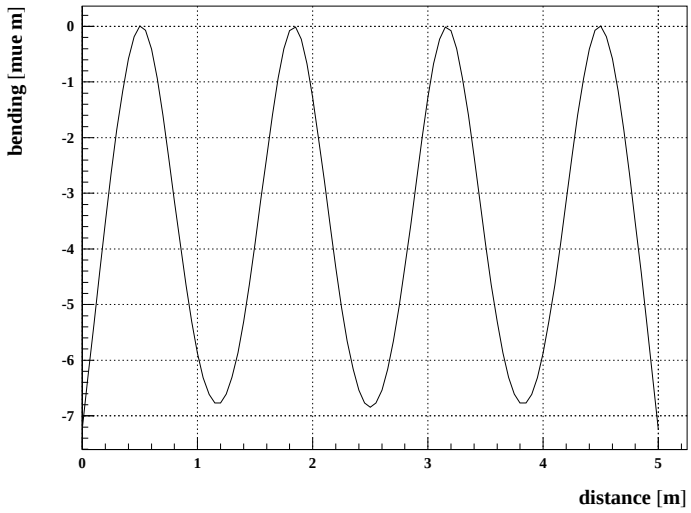

Figure 12: I-beam bending at lowest gap of 12 mm

Assuming aluminium I-beams with a cross section used for the BESSY II IDs the maximum I-beam deflection at a magnetic load of 18 tons (gap of 12 mm) is below 10 μm (fig. 12). This number is a rough guide line based on a 1-dim model and vertical forces only. 3d-FEM calculations are necessary to simulate also the influence of the longitudinal and transverse forces. Thermal gradients inside the

FEL tunnel does not introduce gap fluctuations because the upper and lower I-beams bend into the same direction. Thermal gradients in the assembling hall are more critical because the effects to the upper and lower I-beam may add up (the upper beam will be rotated upside down after mounting the keepers). A rather pessimistic thermal gradient of 0.3 k/m causes a maximum I-beam deflection of 20 μm.

Numerical simulations using these data show that the brilliance reduction of the first harmonic due to I-beam bending (based on magnetic forces and thernal gradients) is negligible This is certainly different for 3rd generation undulators operating at high harmonics or devices with smaller period lengths.

6 Phase Adapting Unit

For gap tunable undulators it is necessary to vary the phase advance between the individual undulator segments. This can be done either by an electromagnetic or a permanent magnet device. The latter one can be realized with a gap drive mechanism or with rotatable magnets. The permanent magnet solution has the advantage of being hysteresis free. At BESSY the optical phases between two UE56 undulator segments are phased with 8 rotatable permament magnets [1]. A similar design with 6 magnets (three above and 3 below the midplane) can be applied to the SASE5 undulator. Based on a remanence of B_r=1.2 Tesla, a magnet width of 80 mm and a smallest vertical gap between the rotatable magnets of 18 mm appropriate magnet diameters are 25 mm (center magnet) and 17.8 mm (outer magnets) and a longitudinal distance of 120 mm provides a maximum phase advance of 3.1 nm which is well above 2π at the lowest energy of 500 eV. fields and trajectory of this device are plotted in fig. 13

The rotary axes can be coupled mechanically in order to minimize the number of motors needed.

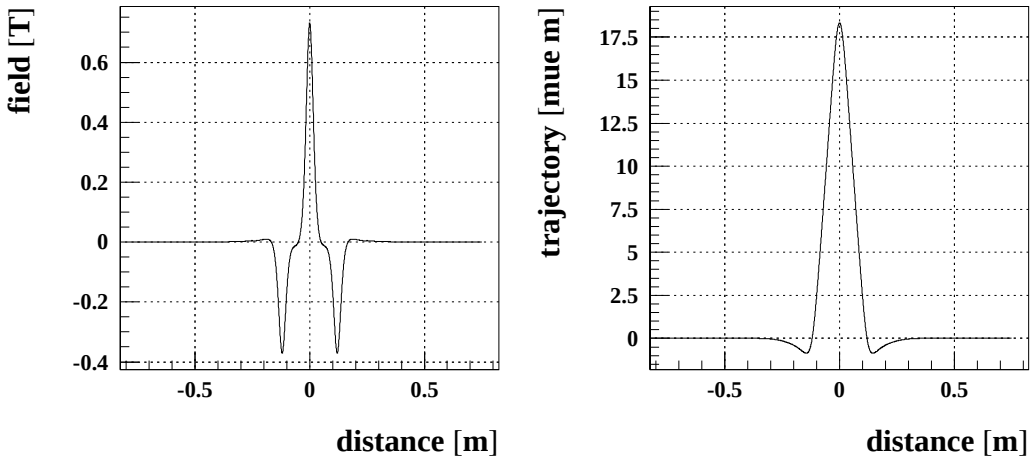

Figure 13: modulator field and trajectory

7 Conclusion

Some technical aspects of an 107 mm period APPLE II undulator for SASE application have been discussed. Technologies developped for 3^{rd} generation light sources are applicable to this device. The required field quality is achievable with appropriate sorting and shimming techniques. The effort on field optimization can certainly be reduced if magnets with better homogeneities could be produced.

References

[1] J. Bahrdt, W. Frentrup, A. Gaupp, M. Scheer, W. Gudat, G. Ingold, S. Sasaki, proceedings of the SRI conference 2000, Berlin, to be published

[2] S. Sasaki, Nucl. Instr. Meth. A347 (1994) 83-86

[3] F.Schäfers, H.-Ch.Mertins, A.Gaupp, W.Gudat, M.Mertin, I.Packe, F.Schmolla, S.DiFonzo, G.Soullie, W.Jark, R.P.Walker, X.LeCann, R.Nyholm, M.Eriksson, Appl.Opt. 38 (1999) 4074-4088

[4] R. Walker, ST/M 97-2, Technical Report ELETTRA (1997)

[5] P. Elleaume, Technical report ESRF/MACH ID 00/59. 2000

[6] P. Elleaume, O. Chubar, J. Chavanne, Proc. of the PAC, Vancouver, Canada, (1997) 3509-3511
O. Chubar, P. Elleaume, J. Chavanne, J. Synchr. Rad. 5 (1998) 481-484

[7] A. Hiraya, K. Yoshida, S. Yagi, M. Taniguchi, S. Kimura, H. Hama, T. Takayama, D. Amano, J. Synchrotron Radiation, 5 (1998) 445-447
S. Kimura, M. Kamada, H. Hama, K. Kimura, M. Hosaka, J. Yamazaki, x.-M. Marechal, T. Tanaka, H. Kitamura, J. Synchrotron Radiation 5 (1998) 453-455
T. Hara, T. Tanaka, T. Tanabe, X.-M. Marechal, K. Kumagai, H. Kitamura, J. Synchrotron Radiation, 5 (1998) 426-427

[8] J. Chavanne, P. Van Varenbergh, P. Elleaume, T. Günzel, Proceedings of the EPAC 2000, Vienna, Austria 2346-2348

[9] J. Chavanne, P. Elleaume, P. Van Varenbergh, proceedings of the PAC 1999, New York, to be published

[10] B. Diviaccio, R. Bracco, D. Millo, R. Walker, M. Zalateu, D. Zangrando, proceedings of the PAC 1999, New York, to be published
S. Marks, J. DeVries, E. Hoyer, B. M. Kincaid, D. Plate, P. Pipersky, R. D. Schlueter, A. Young, proceedings of the PAC 1999, New York, to be published